

## Electronic states in antidot lattices: Scattering-matrix formalism

Seiji Uryu and Tsuneya Ando

*Institute for Solid State Physics, University of Tokyo, 7-22-1 Roppongi, Minato-ku, Tokyo 106, Japan*

(Received 23 October 1995)

A method of full quantum-mechanical calculation of the energy bands with the use of the  $S$  matrix is developed in antidot lattices subjected to a uniform perpendicular magnetic field. It can simplify the calculations considerably in comparison with other methods because only several traveling and a few evanescent modes are sufficient to give accurate results. The resulting energy bands are extremely complicated for realistic antidots. Calculated density of states are analyzed semiclassically in terms of the periodic orbit theory. [S0163-1829(96)06120-6]

### I. INTRODUCTION

Recent advances in microfabrication technology and crystal-growth technique enable one to prepare lateral superlattices with submicrometer structures on the surface of two-dimensional electron system (2DES) with a mean free path of the order of several micrometers. A 2DES modulated by a periodic strong repulsive potential is called "antidot lattices." The transport in this system is ballistic, i.e., electrons are scattered from an antidot potential rather than impurity. The purpose of this paper is to develop a method of full quantum-mechanical calculations of energy bands and conductivity of the antidot lattice in the presence of uniform perpendicular magnetic fields.

Various interesting phenomena have been observed in antidot lattices in uniform perpendicular magnetic fields. They are the quenching of the Hall effect,<sup>1</sup> Al'tshuler-Aronov-Spivak oscillation near  $B \sim 0$ ,<sup>2-4</sup> and the so-called localized peaks in the magnetoresistance.<sup>1</sup> In magnetic fields corresponding to localized peaks, the classical electron trajectory becomes commensurate with the antidot period and encircles a specific number of antidots. Fine oscillations were observed in the magnetoresistance around the localized peak.<sup>5,6</sup>

The localized peaks and the quenching of the Hall effect have been understood in classical mechanics.<sup>1,7</sup> On the fine structures near the localized peak, a semiclassical quantization of periodic orbits was suggested.<sup>6</sup> Semiclassical conductivities have been derived<sup>8</sup> and used for analysis of such fine structures.<sup>9,10</sup> Full quantum-mechanical calculations of energy bands and conductivities were also reported.<sup>11-13</sup> In particular Ishizaka *et al.* made a detailed comparison between semiclassical and full quantum-mechanical results.<sup>13</sup> Transport properties were also calculated by transmission probability through finite number of antidots.<sup>14,15</sup> A method of calculating electronic states and transport properties was developed for finite quantum-dot arrays in high magnetic fields.<sup>16-18</sup>

Difficulties in full quantum-mechanical calculations lie in the fact that the unit cell should be expanded considerably in a magnetic field depending on the flux passing through the unit cell in its absence. In the present  $S$ -matrix formalism we replace the antidot lattice by a two-dimensional array of quantum-wire junctions. Energy bands are determined by imposing Bloch's theorem on an  $S$  matrix that describes the

scattering at a junction. This method can simplify calculations quite effectively by minimizing the necessary number of modes that define the  $S$  matrix. A method to reduce matrix sizes using a recursive Green's-function technique was proposed,<sup>12</sup> but the present method is expected to be much more efficient.

In Sec. II the  $S$ -matrix formalism for the calculation of the energy bands in antidot lattices is described. Some characteristic features of the energy band and their relation to properties of the  $S$  matrix are discussed in Sec. III. Section IV gives results of numerical calculations. The results of electronic states of antidot lattices are analyzed by the periodic orbit theory based on the trace formula in Sec. V. Summary and conclusion are given in Sec. VI. A very preliminary account on a part of this work was presented previously.<sup>19</sup>

### II. S-MATRIX FORMALISM

#### A. $S$ matrix

We shall replace an antidot lattice by a two-dimensional array of quantum-wire junctions as schematically illustrated in Fig. 1. Each junction with the width  $W_x$  in the  $x$  direction and  $W_y$  in the  $y$  direction is connected to neighboring junctions through a quantum wire with length  $L_x$  and  $L_y$  in the  $x$  and  $y$  directions, respectively. The lattice period is  $a$  in the  $x$  direction and  $b$  in the  $y$  direction. The system is subjected to a uniform perpendicular magnetic field  $B$ .

Figure 2 shows a junction of two infinitely long quantum wires. The system is divided into four wires denoted as 1-4 and a rectangular junction region. The origin is chosen at the lower left corner point of the junction. The Hamiltonian for an electron in the two-dimensional  $xy$  plane is

$$\mathcal{H} = \frac{1}{2m^*} \left( \mathbf{p} + \frac{e}{c} \mathbf{A} \right)^2 + V(x, y), \quad (2.1)$$

where,  $m^*$  is the effective mass of electrons,  $V(x, y)$  is the confinement potential, and the vector potential  $\mathbf{A}$  is chosen as

$$\mathbf{A} = (-By, 0). \quad (2.2)$$

It is worth pointing out that the density of states and the conductivity are independent of this choice of the gauge.

The wave functions in the wires 1-4 are given by

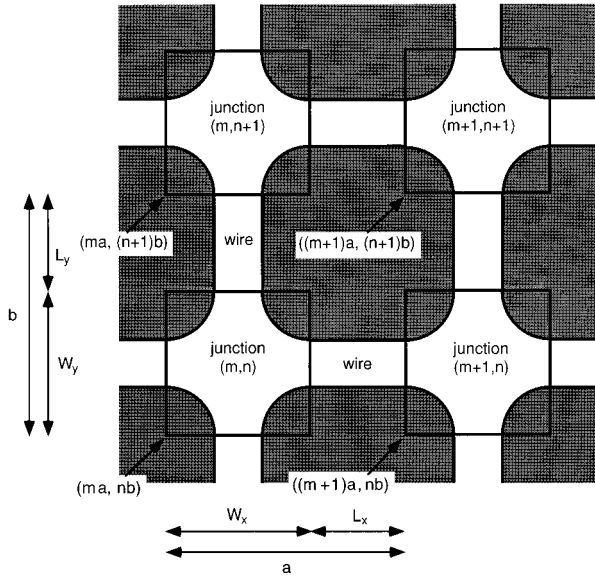


FIG. 1. Schematic illustration of a two-dimensional array of junctions.

$$\psi_{1\nu\pm}^{(0,0)} = \frac{1}{\sqrt{v_\nu^x}} \exp \left[ i \left( \pm \kappa_\nu^x + \frac{W_y}{2l^2} \right) \left( x + \frac{L_x}{2} \right) \right] \eta_{\nu\pm}(y), \quad (2.3)$$

$$\psi_{2\nu\pm}^{(0,0)} = \frac{1}{\sqrt{v_\nu^y}} \exp \left[ i \left( \pm \kappa_\nu^y - \frac{W_x}{2l^2} \right) \left( y + \frac{L_y}{2} \right) \right] \times \exp \left( -i \frac{xy}{l^2} \right) \xi_{\nu\pm}(x),$$

$$\psi_{3\nu\pm}^{(0,0)} = \frac{1}{\sqrt{v_\nu^x}} \exp \left[ i \left( \pm \kappa_\nu^x + \frac{W_y}{2l^2} \right) \left( x - W_x - \frac{L_x}{2} \right) \right] \eta_{\nu\pm}(y),$$

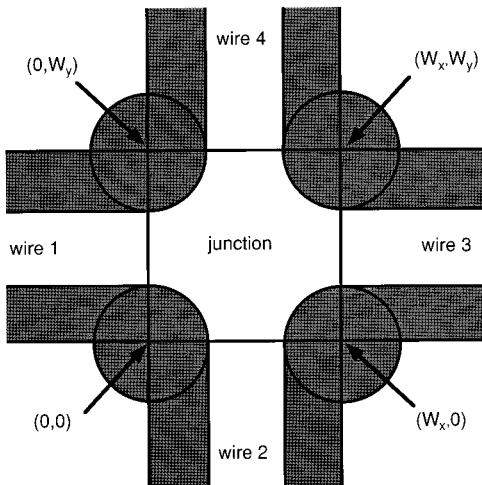


FIG. 2. Schematic illustration of a quantum-wire junction for calculation of an  $S$  matrix.

$$\psi_{4\nu\pm}^{(0,0)} = \frac{1}{\sqrt{v_\nu^y}} \exp \left[ i \left( \pm \kappa_\nu^y - \frac{W_x}{2l^2} \right) \left( y - W_y - \frac{L_y}{2} \right) \right] \times \exp \left( -i \frac{xy}{l^2} \right) \xi_{\nu\pm}(x),$$

where  $l$  is the magnetic length defined by  $l = \sqrt{eB/c\hbar}$ . Modes in each wire are specified as  $\nu\pm$  with integer  $\nu$ . There are two kinds of modes: traveling modes with real wave number and evanescent modes with imaginary wave number. For each  $\nu$ , we shall define the wave number  $\kappa_\nu$  in such a way that it is positive for traveling modes and its imaginary is positive for evanescent modes. The sign  $+$  ( $-$ ) denotes a mode traveling or decaying in the positive (negative) direction with wave number  $\kappa_\nu$  ( $-\kappa_\nu$ ). The wave function is given by  $\eta_{\nu\pm}(y)$  for the motion in the  $y$  direction in a wire infinitely long in the  $x$  direction. In a wire in the  $y$  direction, the corresponding wave function is written as  $\xi(x)$  with the gauge  $\mathbf{A}' = (0, Bx)$ , which is different from Eq. (2.2). They are solutions of the equations

$$\left[ -\frac{\hbar^2}{2m^*} \frac{d^2}{dy^2} + \frac{1}{2} m^* \omega_c^2 (y \mp l^2 \kappa_\nu^x - W_y/2)^2 + V(y) \right] \eta_{\nu\pm}(y) = E \eta_{\nu\pm}(y), \quad (2.4)$$

$$\left[ -\frac{\hbar^2}{2m^*} \frac{d^2}{dx^2} + \frac{1}{2} m^* \omega_c^2 (x \pm l^2 \kappa_\nu^y - W_x/2)^2 + V(x) \right] \xi_{\nu\pm}(x) = E \xi_{\nu\pm}(x),$$

where  $E$  is the energy and  $\omega_c = eB/m^*c$  the cyclotron frequency. Further,  $v_\nu^x$  and  $v_\nu^y$  are the group velocities of a traveling mode in the  $x$  and the  $y$  direction, respectively, and are given by

$$v_\nu^x = \frac{\hbar}{m^*} \int dy \eta_{\nu+}^*(y) \left( \kappa_\nu^x + \frac{W_y}{2l^2} - \frac{y}{l^2} \right) \eta_{\nu+}(y), \quad (2.5)$$

$$v_\nu^y = \frac{\hbar}{m^*} \int dx \xi_{\nu+}^*(x) \left( \kappa_\nu^y - \frac{W_x}{2l^2} + \frac{x}{l^2} \right) \xi_{\nu+}(x).$$

This velocity has been defined in such a way that it is always positive. The normalization factor of an evanescent mode is arbitrary, as will be discussed below. The wave function in wires is represented by using the expansion coefficients  $C$  with respect to modes of Eqs. (2.3):

$$\Psi_i^{(0,0)}(x, y) = \sum_\nu \{ C_{i\nu+}^{(0,0)} \psi_{i\nu+}^{(0,0)}(x, y) + C_{i\nu-}^{(0,0)} \psi_{i\nu-}^{(0,0)}(x, y) \}, \quad (2.6)$$

with  $i=1, \dots, 4$ . The  $S$  matrix gives the following relation between incoming and outgoing waves:

$$\begin{pmatrix} C_{1-}^{(0,0)} \\ C_{2-}^{(0,0)} \\ C_{3+}^{(0,0)} \\ C_{4+}^{(0,0)} \end{pmatrix} = \begin{pmatrix} S_{11} & S_{12} & S_{13} & S_{14} \\ S_{21} & S_{22} & S_{23} & S_{24} \\ S_{31} & S_{32} & S_{33} & S_{34} \\ S_{41} & S_{42} & S_{43} & S_{44} \end{pmatrix} \begin{pmatrix} C_{1+}^{(0,0)} \\ C_{2+}^{(0,0)} \\ C_{3-}^{(0,0)} \\ C_{4-}^{(0,0)} \end{pmatrix}, \quad (2.7)$$

where  $\mathbf{C}$  consists of expansion coefficients  $C$  and therefore its dimension is the number of modes. The  $S$  matrix defined above is not necessarily unitary because evanescent modes do not carry current, although the part of the  $S$  matrix for traveling modes is unitary. For wires connected to a junction specified by  $(m, n)$ , modes  $\nu$  in 1–4 wires are defined by

$$\psi_{i\nu}^{(m,n)}(x,y) = \psi_{i\nu}^{(0,0)}(x-ma, y-nb) \exp\left[-i \frac{nb}{l^2} (x-ma)\right]. \quad (2.8)$$

For this definition, the scattering problem at each quantum-wire junction is described by the same  $S$  matrix.

Kirczenow and collaborators<sup>16–18</sup> developed a method of calculating electronic states and transport properties of dot arrays in high magnetic fields. In this method an  $S$  matrix is defined as a quantity describing mixing between edge channels existing in each dot. The method seems to be quite effective in systems consisting of a periodic array of dots interacting weakly with each other, particularly in high magnetic fields where clear edge states are formed. On the other hand, the present method considers the scattering among states associated with channel regions between neighboring antidots and is expected to be more suitable in antidot lattices consisting of periodic array of “scatterers” instead of dots. The present method and that of Kirczenow and co-workers are considered to be complimentary to each other.

### B. Energy band

For an infinitely large array of such junctions the period is  $a = W_x + L_x$  in the  $x$  direction and  $b = W_y + L_y$  in the  $y$  direction. We restrict our calculation to magnetic fields with a rational number of flux quanta per unit cell, i.e.,  $Bab/\Phi_0 = p/q$ , where  $p$  and  $q$  are mutual prime numbers and we shall impose Bloch’s theorem for the period  $a$  in the  $x$  direction and  $qb$  in the  $y$  direction. An  $S$  matrix  $S_e$  for this extended magnetic unit cell is given from the combination of an  $S$  matrix for a unit cell. We have

$$\begin{pmatrix} \mathbf{C}_1^- \\ \mathbf{C}_2^- \\ \mathbf{C}_3^+ \\ \mathbf{C}_4^+ \end{pmatrix} = \begin{pmatrix} S_{e11} & S_{e12} & S_{e13} & S_{e14} \\ S_{e21} & S_{e22} & S_{e23} & S_{e24} \\ S_{e31} & S_{e32} & S_{e33} & S_{e34} \\ S_{e41} & S_{e42} & S_{e43} & S_{e44} \end{pmatrix} \begin{pmatrix} \mathbf{C}_1^+ \\ \mathbf{C}_2^+ \\ \mathbf{C}_3^- \\ \mathbf{C}_4^- \end{pmatrix}, \quad (2.9)$$

with

$$\mathbf{C}_1^\pm \equiv \begin{pmatrix} \mathbf{C}_{1\pm}^{(m,n+q-1)} \\ \vdots \\ \mathbf{C}_{1\pm}^{(m,n)} \end{pmatrix}, \quad \mathbf{C}_3^\pm \equiv \begin{pmatrix} \mathbf{C}_{3\pm}^{(m,n+q-1)} \\ \vdots \\ \mathbf{C}_{3\pm}^{(m,n)} \end{pmatrix},$$

$$\mathbf{C}_2^\pm \equiv \mathbf{C}_{2\pm}^{(m,n)}, \quad \mathbf{C}_4^\pm \equiv \mathbf{C}_{4\pm}^{(m,n+q-1)}.$$

When  $\mathbf{A} = (-By, 0)$ , Bloch’s theorem is given as follows for this magnetic unit cell:

$$\psi_{k_x, k_y}(x, y) = \exp(-ik_x a) \psi_{k_x, k_y}(x+a, y) \quad (2.10)$$

$$= \exp\left[i\left(\frac{x}{l^2} - k_y\right)qb\right] \psi_{k_x, k_y}(x, y+qb). \quad (2.11)$$

Bloch’s theorem imposes the following conditions on the wave function in the wire region:

$$\Psi_1^{(m,n+i)}(x,y) = \exp(-ik_x a) \Psi_3^{(m,n+i)}(x+a, y) \quad (2.12)$$

for  $ma - L_x \leq x \leq ma$  and  $nb \leq y \leq nb + W_y$  and

$$\Psi_2^{(m,n)}(x,y) = \exp\left[i\left(\frac{x}{l^2} - k_y\right)qb\right] \Psi_4^{(m,n+q-1)}(x, y+qb) \quad (2.13)$$

for  $na \leq x \leq na + W_x$  and  $nb - L_y \leq y \leq nb$ , with  $i=0, 1, \dots, q-1$ . With the aid of the relations

$$\psi_1^{(m,n+i)}(x,y) = \exp\left[i \frac{(n+i)ab}{l^2}\right] \psi_3^{(m,n+i)}(x+a, y), \quad (2.14)$$

$$\psi_2^{(m,n)}(x,y) = \exp\left(i \frac{qb}{l^2} x\right) \psi_4^{(m,n+q-1)}(x, y+qb), \quad (2.15)$$

Bloch’s theorem for expansion coefficients  $C$  is obtained:

$$C_{1\nu^\pm}^{(m,n+i)} = \exp\left[-i\left(k_x + \frac{(n+i)b}{l^2}\right)a\right] C_{3\nu^\pm}^{(m,n+i)}, \quad (2.16)$$

$$C_{2\nu^\pm}^{(m,n)} = \exp(-ik_y qb) C_{4\nu^\pm}^{(m,n+q-1)}. \quad (2.17)$$

These are rewritten in the relation between incoming and outgoing waves:

$$\begin{pmatrix} \mathbf{C}_1^- \\ \mathbf{C}_2^- \\ \mathbf{C}_3^+ \\ \mathbf{C}_4^+ \end{pmatrix} = P_e^{(n)}(k_x, k_y) \begin{pmatrix} \mathbf{C}_1^+ \\ \mathbf{C}_2^+ \\ \mathbf{C}_3^- \\ \mathbf{C}_4^- \end{pmatrix}, \quad (2.18)$$

where

$$P_e^{(n)}(k_x, k_y) = \begin{pmatrix} 0 & 0 & P_x^{-1} & 0 \\ 0 & 0 & 0 & P_y^{-1} \\ P_x & 0 & 0 & 0 \\ 0 & P_y & 0 & 0 \end{pmatrix}, \quad (2.19)$$

with

$$P_x = e^{i(k_x + bn/l^2)a} \begin{pmatrix} e^{i(q-1)ab/l^2} & 0 & \dots & 0 \\ 0 & e^{i(q-2)ab/l^2} & \dots & 0 \\ \dots & \dots & \ddots & \vdots \\ 0 & 0 & \dots & 1 \end{pmatrix},$$

$$P_y = e^{ik_y qb}. \quad (2.20)$$

Energy bands are given by the condition that Eqs. (2.9) and (2.18) have nontrivial solutions of  $\mathbf{C}$ . This condition is

$$\det[P_e^{(n)}(k_x, k_y) S_e(E) - 1] = 0, \quad (2.21)$$

where the relation  $P_e = P_e^{-1}$  is used and  $S_e(E) = (S_{eii'})$  is the  $S$  matrix for extended unit cell defined in Eq. (2.9) for a given energy  $E$ .

At first glance Eq. (2.21) is dependent on the choice of the unit cell  $n$ . However, we have the relation

$$P_e^{(n)}(k_x + 2\pi p/qa, k_y) = P_e^{(n+1)}(k_x, k_y) \quad (2.22)$$

from the definition of the matrix  $P_e$ . Thus the apparent  $n$  dependence corresponds to nothing but the fact that the energy bands are periodic with period  $2\pi/qa$  in the  $k_x$  direction.

The  $S$  matrix has ambiguity concerning the phase of modes and even the amplitude for evanescent modes. We can choose generally the phase such that

$$\begin{aligned} \tilde{\psi}_{1\nu\pm}(x, y) &= e^{i\theta_{\nu\pm}} \psi_{1\nu\pm}(x, y), \\ \tilde{\psi}_{2\nu\pm}(x, y) &= e^{i\phi_{\nu\pm}} \psi_{2\nu\pm}(x, y), \\ \tilde{\psi}_{3\nu\pm}(x, y) &= e^{i\theta_{\nu\pm}} \psi_{3\nu\pm}(x, y), \\ \tilde{\psi}_{4\nu\pm}(x, y) &= e^{i\phi_{\nu\pm}} \psi_{4\nu\pm}(x, y), \end{aligned} \quad (2.23)$$

where  $\theta$  and  $\phi$  are real for traveling modes and are complex for evanescent modes. If an  $S$  matrix is defined by modes Eq. (2.23), then it is transformed into

$$\tilde{S} = U_1 S U_2, \quad (2.24)$$

where

$$U_1 = \begin{pmatrix} U_{\theta_-} & 0 & 0 & 0 \\ 0 & U_{\phi_-} & 0 & 0 \\ 0 & 0 & U_{\theta_+} & 0 \\ 0 & 0 & 0 & U_{\phi_+} \end{pmatrix} \quad (2.25)$$

and

$$U_2 = \begin{pmatrix} U_{\theta_+}^{-1} & 0 & 0 & 0 \\ 0 & U_{\phi_+}^{-1} & 0 & 0 \\ 0 & 0 & U_{\theta_-}^{-1} & 0 \\ 0 & 0 & 0 & U_{\phi_-}^{-1} \end{pmatrix}, \quad (2.26)$$

with

$$[U_{\theta_{\pm}}]_{mn} = e^{i\theta_{m\pm}} \delta_{mn}, \quad [U_{\phi_{\pm}}]_{mn} = e^{i\phi_{m\pm}} \delta_{mn}. \quad (2.27)$$

These matrices  $U_1$  and  $U_2$  have the property

$$U_2^{-1} P_e U_1^{-1} = P_e, \quad (2.28)$$

which immediately leads to the conclusion that the energy spectrum is independent of ambiguity in the phase of an  $S$  matrix, i.e.,

$$\det[P_e(k_x, k_y) \tilde{S}_e(E) - 1] = \det[P_e(k_x, k_y) S_e(E) - 1]. \quad (2.29)$$

It is necessary to transform Eq. (2.21) into more convenient form for numerical calculations of energy bands. From Eq. (2.17),  $\mathbf{C}_2$  and  $\mathbf{C}_4$  satisfy Bloch's theorem

$$\begin{pmatrix} \mathbf{C}_2^- \\ \mathbf{C}_4^+ \end{pmatrix} = \begin{pmatrix} 0 & P_y^{-1} \\ P_y & 0 \end{pmatrix} \begin{pmatrix} \mathbf{C}_2^+ \\ \mathbf{C}_4^- \end{pmatrix}. \quad (2.30)$$

Substituting Eq. (2.30) into Eq. (2.9), we have

$$\begin{pmatrix} \mathbf{C}_1^- \\ \mathbf{C}_3^+ \end{pmatrix} = \begin{pmatrix} M_{11} & M_{12} \\ M_{21} & M_{22} \end{pmatrix} \begin{pmatrix} \mathbf{C}_1^+ \\ \mathbf{C}_3^- \end{pmatrix}, \quad (2.31)$$

with

$$\begin{aligned} \begin{pmatrix} M_{11} & M_{12} \\ M_{21} & M_{22} \end{pmatrix} &\equiv \begin{pmatrix} S_{e11} & S_{e13} \\ S_{e31} & S_{e33} \end{pmatrix} + \begin{pmatrix} S_{e12} & S_{e14} \\ S_{e32} & S_{e34} \end{pmatrix} \\ &\times \begin{pmatrix} -S_{e22} & P_y^{-1} - S_{e24} \\ P_y - S_{e42} & -S_{e44} \end{pmatrix}^{-1} \begin{pmatrix} S_{e21} & S_{e23} \\ S_{e41} & S_{e43} \end{pmatrix}. \end{aligned} \quad (2.32)$$

We then have

$$\begin{pmatrix} \mathbf{C}_3^+ \\ \mathbf{C}_1^- \end{pmatrix} = \begin{pmatrix} 0 & -M_{12} \\ 1 & -M_{22} \end{pmatrix}^{-1} \begin{pmatrix} M_{11} & -1 \\ M_{12} & 0 \end{pmatrix} \begin{pmatrix} \mathbf{C}_1^+ \\ \mathbf{C}_3^- \end{pmatrix}. \quad (2.33)$$

With use of Eq. (2.16), we have the eigenequation

$$\begin{aligned} e^{ik_x a} \begin{pmatrix} \mathbf{C}_1^+ \\ \mathbf{C}_1^- \end{pmatrix} &= \begin{pmatrix} P_x^{-1} & 0 \\ 0 & P_x^{-1} \end{pmatrix} \begin{pmatrix} 0 & -M_{12} \\ 1 & -M_{22} \end{pmatrix}^{-1} \begin{pmatrix} M_{11} & -1 \\ M_{12} & 0 \end{pmatrix} \\ &\times \begin{pmatrix} \mathbf{C}_1^+ \\ \mathbf{C}_1^- \end{pmatrix}. \end{aligned} \quad (2.34)$$

Therefore,  $k_x$  can be calculated for a given  $E$  and  $k_y$  from eigenvalues of Eq. (2.34). Similarly,  $k_y$  can be calculated for a given  $E$  and  $k_x$ . This simplifies greatly the actual calculation for the energy band, because the calculation of the determinant is quite time consuming.

### C. Density of states and conductivity

The density of states and conductivity can be calculated from energy bands. The density of states  $D(E)$  is written as

$$D(E) = \frac{2}{(2\pi)^2} \oint \frac{dl}{\hbar|\mathbf{v}|}, \quad (2.35)$$

where 2 comes from the spin degeneracy and the line integral is along the equienergy line at energy  $E$ . The group velocity  $\mathbf{v}$  is

$$\mathbf{v}(k) = \frac{1}{\hbar} \frac{\partial E(\mathbf{k})}{\partial \mathbf{k}}. \quad (2.36)$$

The conductivity can be calculated with use of the Boltzmann transport equation and becomes

$$\sigma_{ij} = \frac{1}{2\pi^2} \int \oint \frac{e^2 \tau v_i v_j}{\hbar|\mathbf{v}|} \left( -\frac{\partial f}{\partial E} \right) dl dE, \quad (2.37)$$

where  $f$  is the Fermi distribution function,  $\tau$  is a phenomenological relaxation time,  $i, j = x, y$ , and the line integral is along the equienergy line. Unfortunately, Eq. (2.37) gives only the symmetric part of the conductivity tensor, i.e.,  $\sigma_{xy} = \sigma_{yx}$ , and an antisymmetry part or the Hall conductivity cannot be obtained from this equation.

### III. SOME EXAMPLES

#### A. Single traveling mode

We consider the simplest case of a square antidot with a single traveling channel in the absence of a magnetic field. The  $S$  matrix is written as

$$S(E) = \begin{pmatrix} r & s & t & s \\ s & r & s & t \\ t & s & r & s \\ s & t & s & r \end{pmatrix}, \quad (3.1)$$

where  $r$  is the reflection amplitude,  $s$  is the transmission amplitude for turning left or right, and  $t$  is that for going straight. Usually,  $r$ ,  $s$ , and  $t$  are complex numbers and satisfy the relations from the unitarity of an  $S$  matrix

$$\begin{aligned} |r|^2 + 2|s|^2 + |t|^2 &= 1, \\ \text{Re}[(r+t)s^*] &= 0, \end{aligned} \quad (3.2)$$

$$|s|^2 + \text{Re}[rt^*] = 0.$$

Subtracting twice the third equation of Eq. (3.2) from the first one yields the relation

$$|r-t| = 1. \quad (3.3)$$

Equation (2.21) yields

$$4\alpha \cos(k_x a) \cos(k_y a) + 2\beta [\cos(k_x a) + \cos(k_y a)] + \gamma = 0, \quad (3.4)$$

with

$$\begin{aligned} \alpha &= t^2 - s^2, \\ \beta &= 2s^2(t-r) + t(r^2 - 1 - t^2), \\ \gamma &= -4s^2(t-r)^2 + (r^2 - 1 - t^2)^2. \end{aligned} \quad (3.5)$$

It is straightforward to show with the use of the unitarity condition (3.2) that Eq. (3.4) constitutes a single equation, i.e., the real and imaginary parts give the same equation.

We can derive characteristic features of the bands using Eqs. (3.4) and (3.5). The following are some examples.

(i) For an energy where  $r-t=-1$ , in particular, Eq. (3.4) becomes  $[\cos(k_x a) - 1][\cos(k_y a) - 1] = 0$ , giving the equienergy line  $k_x = 0$  or  $k_y = 0$ .

(ii) For an energy where  $r-t=1$ , on the other hand, Eq. (3.4) becomes  $[\cos(k_x a) + 1][\cos(k_y a) + 1] = 0$ , giving the equienergy line  $k_x = \pi/a$  or  $k_y = \pi/a$ .

(iii) Finally, when  $t^2 \approx s^2 \approx 0$  and  $|r|^2 \approx 1$ , Eq. (3.4) gives  $\cos(k_x a) + \cos(k_y a) = (1-r^2)/2t$ . This seldom has a solution because  $t$  is very small unless  $r = \pm 1$ , leading to the formation of a gap at this energy.

These peculiar features can be found in the numerical results given in Sec. IV A.

#### B. Single evanescent mode

Consider the case that an  $S$  matrix defined with a single evanescent mode is sufficient for accurate description of the system. Then we can choose the phase of wave functions

such that  $r$ ,  $s$ , and  $t$  are all real without loss of generality. When the energy is close to a quasibound level  $E_0$  localized inside a junction, we have

$$r \approx \pm s \approx t \approx -\frac{t_0}{E-E_0}, \quad (3.6)$$

with  $t_0$  being a constant having the dimension of energy. This leads to  $\alpha \sim 0$ ,  $\beta \sim -t$ , and  $\gamma \sim 1$ . Therefore, the energy band becomes

$$E = E_0 - 2t_0[\cos(k_x a) + \cos(k_y a)], \quad (3.7)$$

which is nothing but the band obtained in a nearest-neighbor tight-binding model.

When the energy is close at a quasibound level  $E_1$  associated with the first excited one-dimensional (1D) subband, on the other hand, an  $S$  matrix for the evanescent mode with the smallest wave number is written as

$$S(E) = \begin{pmatrix} r & s & t & -s \\ s & r & -s & t \\ t & -s & r & s \\ -s & t & s & r \end{pmatrix}, \quad (3.8)$$

because of the symmetry of the wave function,<sup>20</sup> and we have

$$r \approx \pm s \approx -t \approx -\frac{t_1}{E-E_1}, \quad (3.9)$$

with  $t_1$  being a constant. Then the energy band is

$$E = E_1 + 2t_1[\cos(k_x a) + \cos(k_y a)], \quad (3.10)$$

which is again a band obtained in a nearest-neighbor tight-binding model.

## IV. NUMERICAL RESULTS

### A. $S$ matrix in a lattice model

To calculate an  $S$  matrix for a quantum-wire junction we consider a two-dimensional system on a square lattice with lattice constant  $a'$  and an isotropic nearest-neighbor transfer integral. The magnetic field is included in terms of a Peierls phase factor of the transfer integral and the confinement potential is included as a local site energy. This lattice model can simulate the two-dimensional system at GaAs/Al<sub>x</sub>Ga<sub>1-x</sub>As heterostructures well if we choose the lattice constant such that  $\lambda_F a' \geq 10$  with  $\lambda_F$  is the Fermi wavelength of the 2DES in the absence of the antidot potential. The  $S$  matrix is calculated in a recursive Green's-function technique developed previously.<sup>21</sup> In order to demonstrate the accuracy of the  $S$ -matrix method, we shall calculate also exact energy bands by diagonalizing the Hamiltonian in the same lattice model.

Although an antidot potential should be determined by a self-consistent calculation,<sup>22,23</sup> we use the model potential  $V(x, y)$  given by<sup>7</sup>

$$V(x, y) = U_0 \left[ \cos\left(\frac{\pi x}{a}\right) \cos\left(\frac{\pi y}{a}\right) \right]^{2\beta}, \quad (4.1)$$

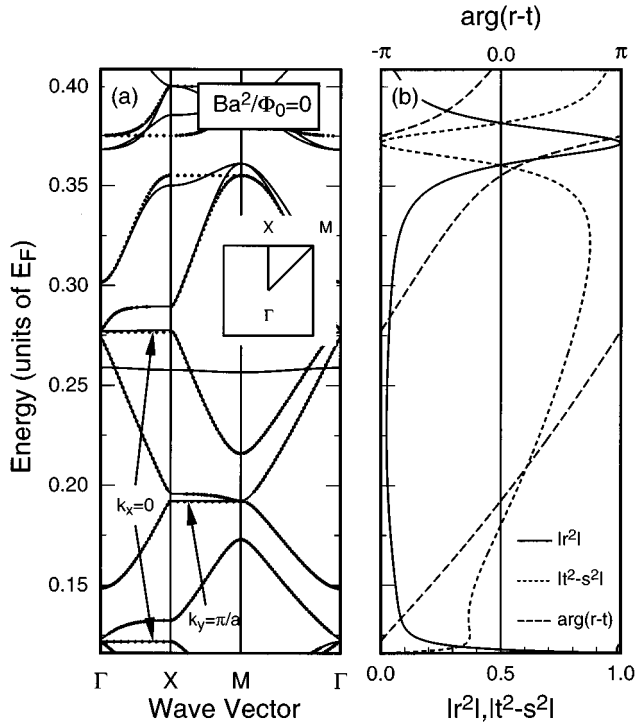


FIG. 3. (a) Calculated energy bands of antidot lattices in the absence of magnetic fields in the energy with a single traveling mode and (b) energy dependence of  $|r^2|$ ,  $|t^2 - s^2|$ , and  $\arg(r-t)$ . The dots are calculated by using the  $S$  matrix with the inclusion of a single traveling mode and solid lines by diagonalizing directly the Hamiltonian of the lattice model. The inset shows the first Brillouin zone.

where  $U_0$  is a maximum of the potential,  $\beta$  is a parameter describing steepness of potential, and  $a$  is the period. This potential corresponds to the system where  $L_x = L_y = 0$  and  $W_x = W_y = a$  in Fig. 1. It is convenient to introduce the antidot diameter  $d$  defined as the width in the  $x$  direction of the region where the antidot potential is larger than the Fermi energy  $E_F$ . In the following numerical calculations we shall choose the parameters such that  $a/\lambda_F = 4.31$ ,  $U_0/E_F = 8.4$ ,  $d/a = 0.6$ , and  $\beta = 2$ . Further, the energy is measured in units of the Fermi energy in the absence of antidot potential.

### B. Single traveling or evanescent case

Figure 3(a) shows energy bands in the energy region corresponding to the presence of a single traveling mode ( $0.166 < E/E_F < 0.409$ ) in the absence of a magnetic field. The dots represent the bands calculated by including only a traveling mode in the  $S$ -matrix method and the solid lines those obtained by a direct diagonalization of the Hamiltonian in a lattice model. The  $S$ -matrix results are in good agreement with the exact results except in the high-energy region near the bottom of the first excited 1D subband. Further, the narrow band at  $E/E_F \sim 0.258$ , which is the quasi-bound level associated with the first excited 1D subband, is absent in the  $S$ -matrix results. As will be demonstrated in Sec. IV C, this discrepancy is removed almost completely if just a single evanescent mode associated with the first excited 1D subband is included. Figure 3(b) shows the corresponding en-

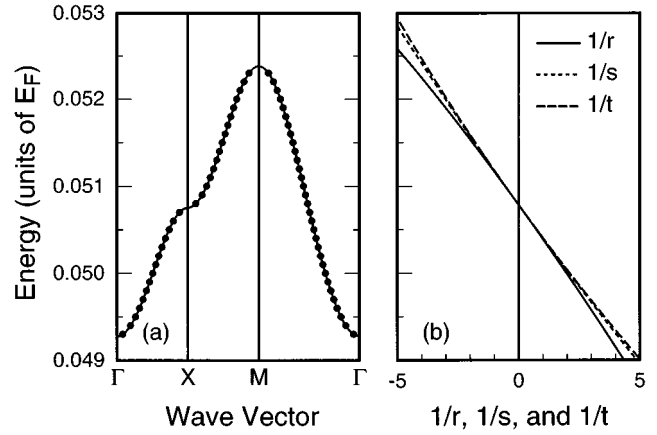


FIG. 4. (a) Narrow band calculated with a single evanescent mode below the bottom of the lowest 1D subband in the wire region and (b) the energy dependence of  $r^{-1}$ ,  $s^{-1}$ , and  $t^{-1}$ .

ergy dependence of  $|r^2|$ ,  $|t^2 - s^2|$ , and  $\arg(r-t)$ , where  $r$ ,  $s$ , and  $t$  are the elements of the  $S$  matrix for the traveling mode, defined in Eq. (3.1).

Almost all the characteristic features of the energy band discussed in Sec. III A appear in the energy bands calculated in the  $S$ -matrix formalism.

(i) The phase of  $r-t$  becomes  $\pm\pi$  or  $r-t = -1$  at the energy  $E/E_F \sim 0.121$ ,  $0.277$ , and  $0.375$  (note that  $|r-t| = 1$  because of the unitarity of the  $S$  matrix). At these energies we have  $k_x = 0$  and  $k_y = 0$ , according to the discussion in Sec. III A.

(ii) Similarly, the phase of  $r-t$  vanishes or  $r-t = 1$  at  $E/E_F \sim 0.192$  and  $0.355$  for which  $k_x = \pm\pi/a$  and  $k_y = \pm\pi/a$ .

(iii) Further,  $|t^2 - s^2| = 0$  and  $|r|^2 \sim 1$  at  $E/E_F \sim 0.372$ , leading to the gap formation. Note that  $|s| \sim 0$  and  $|t| \sim 0$  also at the bottom of the 1D channel  $E/E_F \sim 0.116$ , where the gap is not necessarily formed because  $r \sim 1$ .

Figure 4(a) shows a narrow band at  $E/E_F \sim 0.051$  below the bottom of the lowest 1D subband. This is associated with a bound state formed inside each quantum-wire junction and has the dispersion characteristic to a nearest-neighbor tight-binding model, i.e.,  $\propto [\cos(k_x a) + \cos(k_y a)]$ . Figure 4(b) shows  $1/r$ ,  $1/s$ , and  $1/t$  as a function of energy, where  $r$ ,  $s$ , and  $t$  are the elements of the  $S$  matrix for an evanescent mode. It is clear that this is nothing but a demonstration of the discussion in Sec. III B.

### C. Multichannel case

Figure 5(a) shows the energy bands in the wider energy range. The bands at a given energy are calculated by including all traveling modes and a single evanescent mode having the smallest wave number. The horizontal dotted lines denote the bottom of 1D subbands in the wire region. The results by using the  $S$ -matrix formalism and diagonalizing the Hamiltonian agree well with each other. In particular the disagreement existing in Fig. 3 disappeared completely. This shows that the  $S$  matrix including a few evanescent modes in addition to all traveling modes is sufficient for accurate description of energy bands of antidot lattices.

Figure 5(b) gives the results in a magnetic field  $Ba^2/\Omega_0 = 4$ , which corresponds to about 0.4 T for a typical

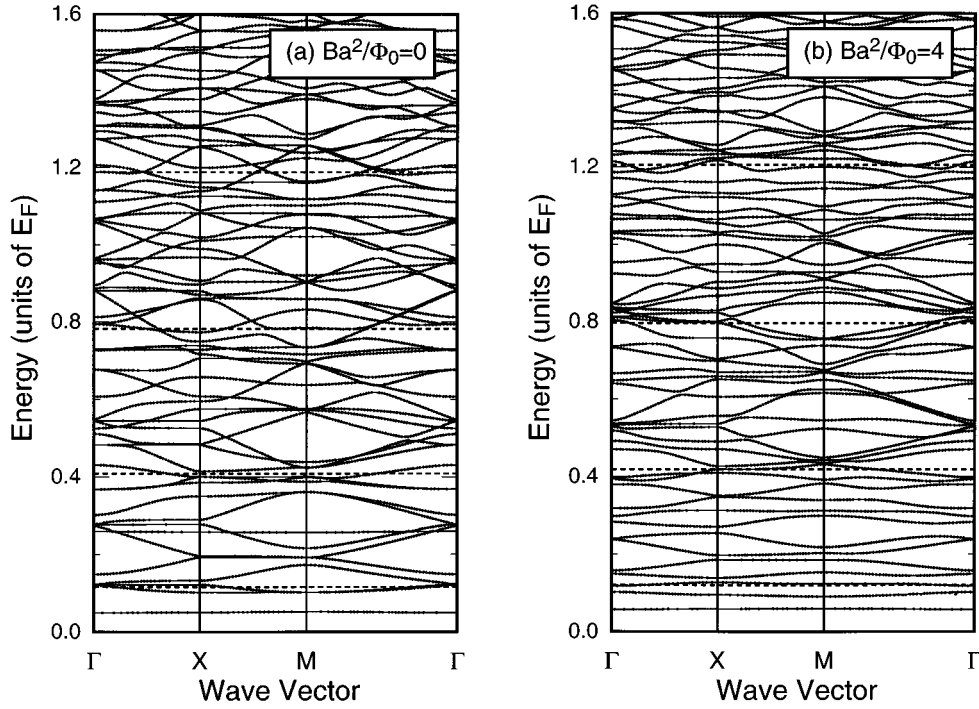


FIG. 5. Calculated energy bands (a) in the absence of a magnetic field and (b) in a magnetic field  $Ba^2/\Phi_0=4$ . In the  $S$ -matrix method, all traveling modes and only a single evanescent mode are taken into account.

antidot lattice with  $a \sim 2000 \text{ \AA}$ . The agreement of the results of the  $S$ -matrix formalism with exact ones is again excellent. Unfortunately, the energy bands of a realistic antidot lattice are very complicated. It is very difficult, therefore, to discuss its electronic properties directly based on the band structure alone.

The exact diagonalization of the Hamiltonian matrix for such a realistic antidot lattice must deal with a matrix of dimension ( $\sim 1000, \sim 1000$ ) even in the absence of a magnetic field or a special magnetic field corresponding to the case that the flux passing through a unit cell is an integer multiple of the flux quantum. This shows that such a calculation is actually impossible in magnetic fields, which require a considerably extended magnetic unit cell. The present  $S$ -matrix formalism does not have such a severe restriction and is quite useful.

Figures 6(a) and 6(b) show the corresponding energy dependence of the density of states and the conductivity. The density of states is measured in units of the 2DES value  $m^*/\pi\hbar^2$  and the conductivity in units of  $ne^2\tau/m^*$ , with  $n$  being the electron concentration in the absence of antidot potential. They are averaged over the Gaussian distribution with broadening  $\Gamma/E_F=0.02$ . The peaks of the density of states remaining after the average may correspond to classical periodic orbits and be analyzed semiclassically in terms of Gutzwiller's trace formula.<sup>24</sup> Some of structures of the

conductivity correspond to those of the density of states, but there are some differences from those of the density of states. This shows that the analysis of the density of states is insufficient for understanding oscillations of the conductivity appearing in antidot lattices.

## V. SEMICLASSICAL ANALYSIS

### A. Trace formula

According to Gutzwiller's trace formula,<sup>24</sup> the density of states of a chaotic system is given semiclassically by the contribution of classical periodic orbits as

$$D(E) = D_0(E) + \sum_{\text{PO}} D_{\text{osc}}^{\text{PO}}(E), \quad (5.1)$$

where  $D_0(E)$  is the mean density of states and  $D_{\text{osc}}^{\text{PO}}(E)$  is the oscillatory part. The contribution of a particular periodic orbit can be rewritten into the  $\delta$  function for a stable orbit

$$D_{\text{osc}}^{\text{PO}}(E) = \frac{T}{\hbar} \sum_{m=0}^{\infty} \left[ \sum_{n=-\infty}^{\infty} \delta(S_c/\hbar - (m + \frac{1}{2})v - 2n\pi) - \frac{1}{2\pi} \right] \quad (5.2)$$

and into Lorentzian for an unstable orbit

$$D_{\text{osc}}^{\text{PO}}(E) = \frac{T}{\hbar} \sum_{m=0}^{\infty} (\pm 1)^m \left[ \sum_{n=-\infty}^{\infty} \frac{1}{\pi} \frac{(2m+1)u/2}{[S_c/\hbar - 2\pi(\mu/4+n)]^2 + [(2m+1)u/2]^2} - \frac{1}{2\pi} \right], \quad (5.3)$$

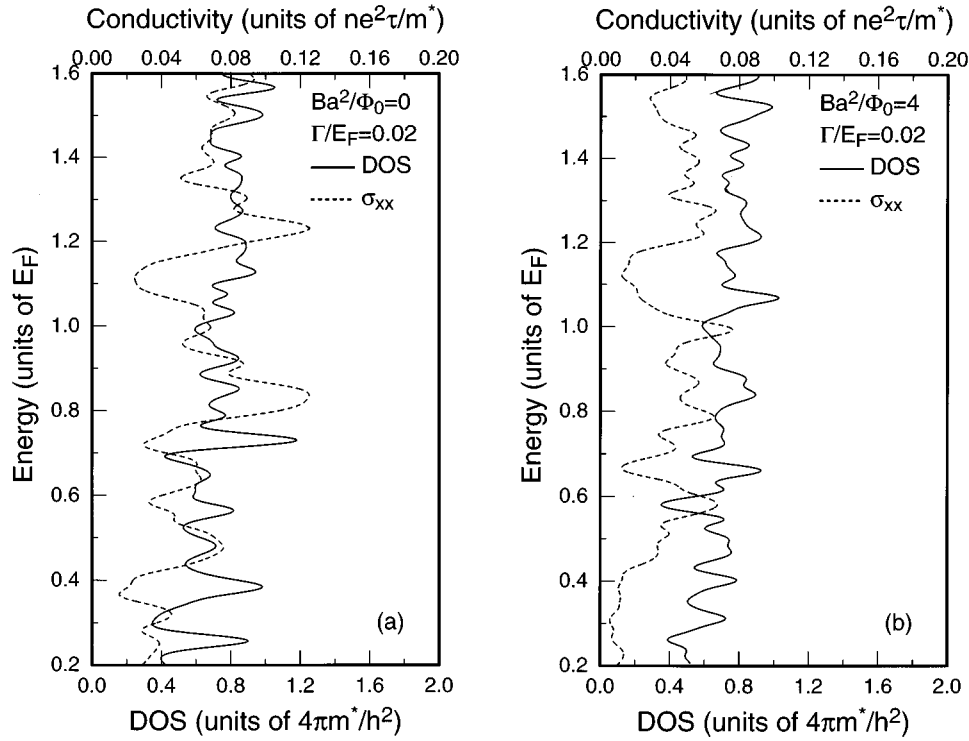


FIG. 6. Energy dependence of the density of states (solid line) and the conductivity (dotted line) (a) in the absence of a magnetic field and (b) in the magnetic field  $Ba^2/\Phi_0=4$ . The density of states is normalized by the 2D value ( $4\pi m^*/h^2$ ) and the conductivity by the value ( $ne^2\tau/m^*$ ). Both are averaged by a Gaussian distribution with broadening  $\Gamma/E_F=0.02$ .

where  $S_c$  is the classical action,  $T$  is the period, and  $v$  is the stability angle. For unstable orbits,  $u$  is the Lyapunov exponent,  $\mu$  is the Maslov index, and the sign becomes  $\pm$  accordingly as the neighborhood of a periodic orbit is hyperbolic or inverse hyperbolic. The integer  $m$  is considered as a quantum number for a motion transverse to the periodic orbit.<sup>25</sup> The quantization conditions for stable and unstable orbits are

$$S_c = \begin{cases} 2\pi\hbar \left\{ n + \frac{1}{2\pi} \left( m + \frac{1}{2} \right) v \right\} & \text{for stable orbit} \\ 2\pi\hbar \left( n + \frac{\mu}{4} \right) & \text{for unstable orbit,} \end{cases} \quad (5.4)$$

with integer  $n$  and positive integer  $m$ .

### B. Numerical results

In general, a long periodic orbit is expected to have a large Lyapunov exponent  $u$  and give only a small contribution to the oscillatory density of states. Therefore, we shall take into account several periodic orbits having shortest trajectory denoted as (a)–(f) shown in Fig. 7.<sup>9</sup> Figure 7(a) shows orbits in the absence of a magnetic field and Fig. 7(b) those for  $Ba^2/\Phi_0=8.5$ , where the cyclotron diameter is nearly equal to the antidot period. The density of states is calculated by taking into account terms with  $m=0$  alone.<sup>26</sup>

Figure 8 compares the oscillatory part of the density of states in the absence of the magnetic field. The solid line denotes the results calculated by using the  $S$ -matrix formalism and by subtracting the average and the dotted line is calculated with periodic orbit theory. Both results are averaged over the Gaussian distribution with broadening

$\Gamma/E_F=0.03$ . The arrows indicate the quantization levels of each periodic orbit. Figure 9 gives calculated Lyapunov exponents for the periodic orbits (a)–(f), which show that almost all periodic orbits are unstable in the energy range

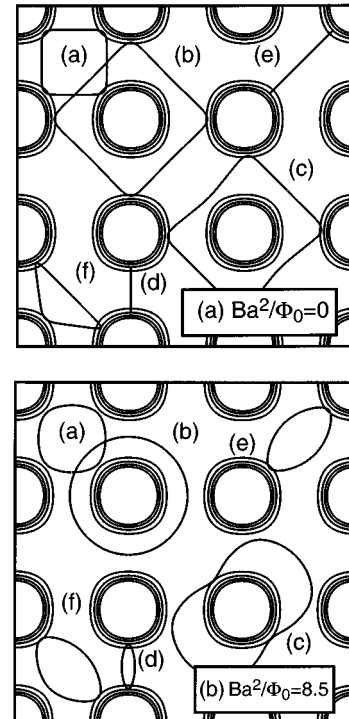


FIG. 7. Example of periodic orbits in an antidot lattice (a) in the absence of a magnetic field and (b) in the magnetic field  $Ba^2/\Phi_0=8.5$ .

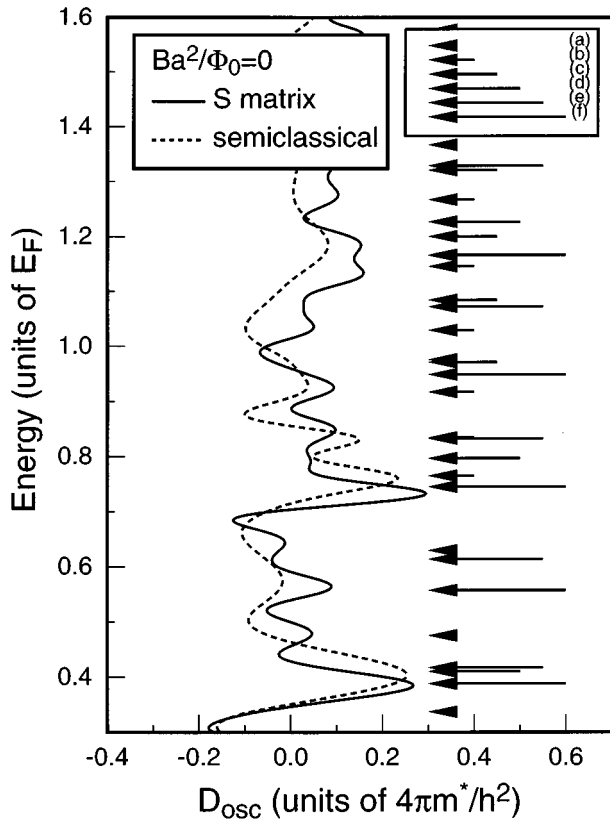


FIG. 8. Oscillator part of the density of states in the absence of a magnetic field. The solid line is calculated with  $S$ -matrix formalism and the dotted line the trace formula. Both are averaged by a Gaussian distribution with  $\Gamma/E_F=0.03$ .

shown in the figure. The only exception is the orbit (b), which is stable and gives a large contribution in the energy range  $0.76 < E/E_F < 0.85$ .

The peaks of the semiclassical result at the energy

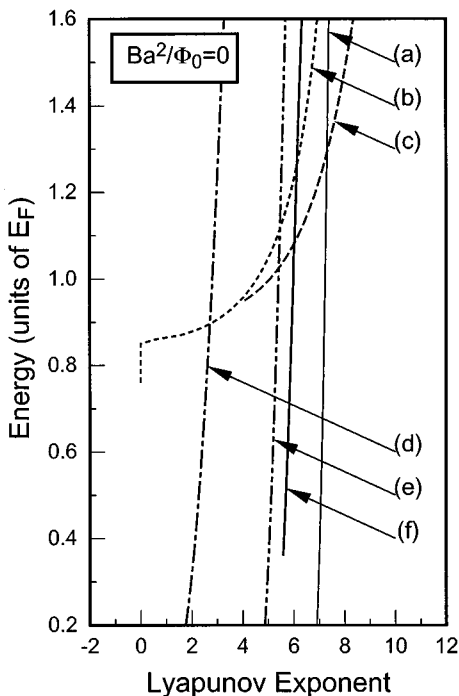


FIG. 9. Calculated Lyapunov exponents of several periodic orbits in the absence of a magnetic field.

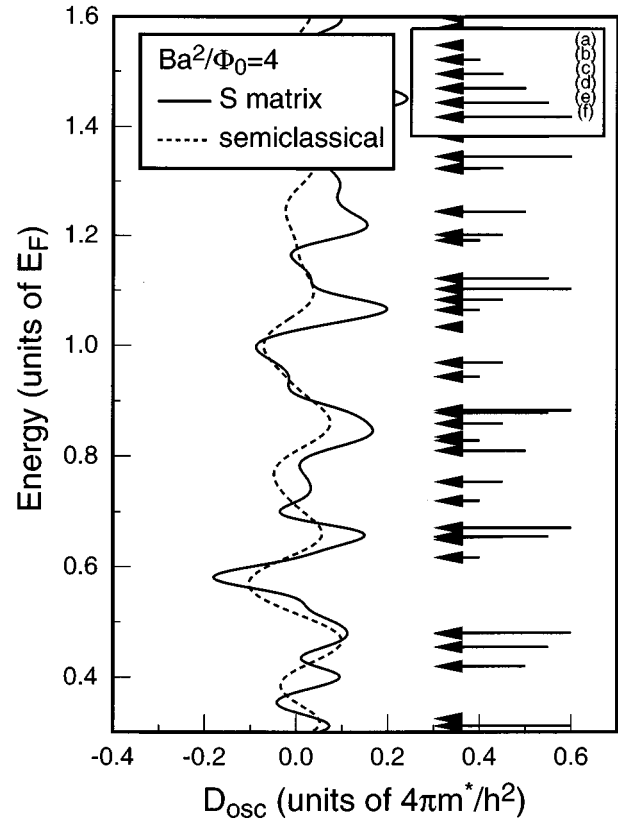


FIG. 10. Oscillator part of the density of states in the magnetic field  $Ba^2/\Phi_0=4$ .

$E/E_F=0.40, 0.57, 0.76, 0.83,$  and  $0.93$  correspond well to those of the full quantum-mechanical density of states. There remain several structures that cannot be reproduced in the semiclassical calculation. The agreement is worse in particular in the energy region higher than the Fermi energy, where periodic orbits more complicated and having a longer trajectory are likely to have a large contribution.

Figure 10 shows the results in the magnetic field  $Ba^2/\Phi_0=4$  for which the periodic orbits (a)–(f) are all unstable in the energy range as shown in Fig. 11. Some of the peaks obtained quantum mechanically are explained again by the periodic orbits but certainly not completely.

Figure 12 gives the results for  $Ba^2/\Phi_0=8.5$ , where the cyclotron orbit is nearly commensurate with the antidot potential. They are averaged over the Gaussian distribution with broadening  $\Gamma/E_F=0.02$ . The agreement between the quantum-mechanical and semiclassical results is much better than in previous two cases, i.e., Figs. 8 and 10. Figure 13 shows the corresponding Lyapunov exponents. The orbit (a) is stable in the energy region below  $E/E_F=0.43$ , the orbit (b) below  $E/E_F=1.41$ , and orbit (e) below  $E/E_F=0.68$ . It is clear that the quantized levels associated with stable periodic orbits (denoted by arrows) can give peaks in the density of states in agreement with the quantum-mechanical result.

The stability of an orbit usually depends strongly on the potential parameters. When  $d/a < 0.66$ , however, the orbit (b) is stable independent of steepness  $\beta$ . This means that the orbit (b) is not affected strongly by fluctuations of antidot potential inherent to actual antidots fabricated experimen-

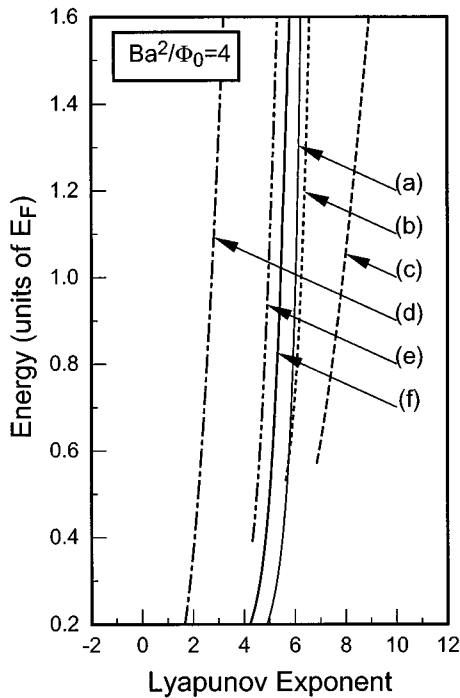


FIG. 11. Calculated Lyapunov exponents of several periodic orbits in the magnetic field  $Ba^2/\Phi_0=4$ .

tally. Therefore the orbit (b) dominates the structures of the density of states near the Fermi energy around the localized or commensurate peaks of the resistivity,<sup>6,10,13</sup> leading to the Aharonov-Bohm-type oscillation observed experimentally.<sup>5,6</sup>

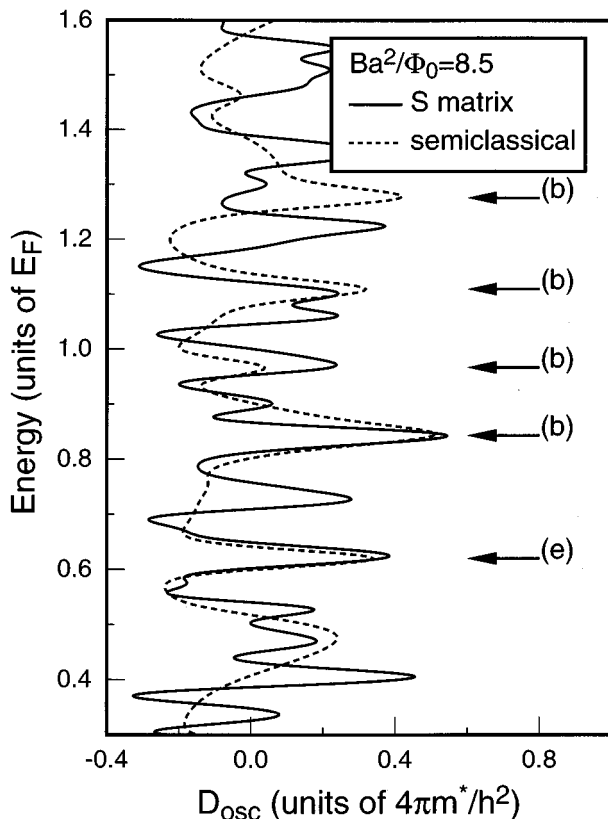


FIG. 12. Oscillator part of the density of states in the magnetic field  $Ba^2/\Phi_0=8.5$  averaged by a Gaussian distribution with  $\Gamma/E_F=0.02$ .

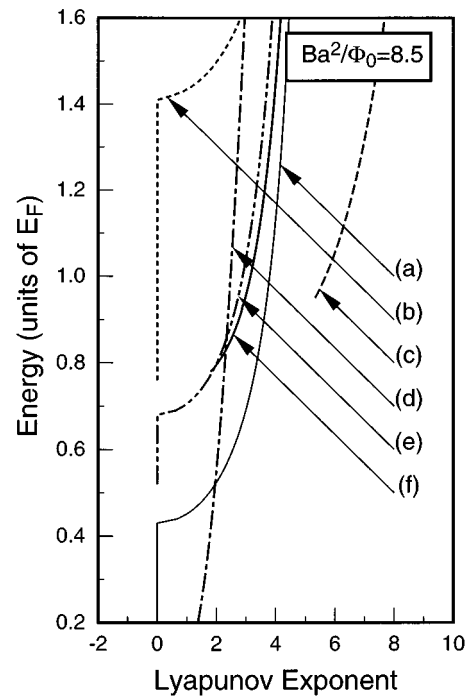


FIG. 13. Calculated Lyapunov exponents of several periodic orbits in the magnetic field  $Ba^2/\Phi_0=8.5$ .

## VI. SUMMARY AND CONCLUSION

We have developed the numerical method of the quantum-mechanical calculation of the electronic states of the antidot lattices in magnetic fields with use of an  $S$  matrix. The method can simplify calculations quite effectively in comparison with the conventional one because the inclusion of traveling modes and only a few evanescent modes is sufficient to reproduce the band structure. It has certainly some limitations such as difficulty in the calculation of the Hall conductivity in strong magnetic fields as well as the eigen-wave functions.

Based on the results of full quantum-mechanical calculations of electronic states, the density of states and the conductivity have been calculated. It has been shown that there is no clear one-to-one correspondence between the peaks and dips of the density of states and the conductivity. The density of states has been calculated semiclassically based on Gutzwiller's trace formula with inclusion of several periodic orbits with shortest trajectory. It is shown that quantized levels associated with these periodic orbits can account for most of peaks in the density of states in magnetic fields where the classical cyclotron orbit is commensurate with the antidot period. Near the Fermi level, in particular, the orbit circling around an antidot gives a major contribution in agreement with the premise of previous analyses.<sup>6,10,13</sup>

## ACKNOWLEDGMENTS

We would like to thank Professor M. Ueda, S. Ishizaka, Dr. T. Nakanishi, H. Ajiki, and K. Asano for useful discussion. This work was supported in part by Grant-in-Aid for Scientific Research on Priority Area "Mesoscopic Electronics: Physics and Technology" from the Ministry of Education, Science and Culture.

- <sup>1</sup>D. Weiss, M. L. Roukes, A. Menschig, P. Grambow, K. von Klitzing, and G. Weimann, *Phys. Rev. Lett.* **66**, 2790 (1991).
- <sup>2</sup>G. M. Gusev, Z. D. Kvon, L. V. Litvin, Yu. V. Nastaushev, A. K. Kalagin, and A. I. Toropov, *Pis'ma Zh. Eksp. Teor. Fiz.* **55**, 129 (1991) [*JETP Lett.* **55**, 123 (1992)].
- <sup>3</sup>K. Nakamura, S. Ishizaka, and F. Nihey, *Physica B* **197**, 144 (1994).
- <sup>4</sup>F. Nihey, S. W. Hwang, and K. Nakamura, *Phys. Rev. B* **51**, 4649 (1995).
- <sup>5</sup>F. Nihey and K. Nakamura, *Physica B* **184**, 398 (1993).
- <sup>6</sup>D. Weiss, K. Richter, A. Menschig, R. Bergmann, H. Schweizer, K. von Klitzing, and G. Weimann, *Phys. Rev. Lett.* **70**, 4118 (1993).
- <sup>7</sup>R. Fleischmann, T. Geisel, and R. Ketzmerick, *Phys. Rev. Lett.* **68**, 1367 (1992); *Europhys. Lett.* **25**, 219 (1994).
- <sup>8</sup>M. Wilkinson, *J. Phys. A* **20**, 2415 (1987).
- <sup>9</sup>K. Richter, *Europhys. Lett.* **29**, 7 (1995).
- <sup>10</sup>G. Hackenbroich and F. von Oppen, *Europhys. Lett.* **29**, 151 (1995).
- <sup>11</sup>H. Silberbauer, *J. Phys. Condens. Matter* **4**, 7355 (1992); H. Silberbauer and U. Rösler, *Phys. Rev. B* **50**, 11 911 (1994).
- <sup>12</sup>R. B. S. Oakshott and A. MacKinnon, *J. Phys. Condens. Matter* **5**, 6971 (1993); **5**, 6983 (1993); **5**, 6991 (1993); **6**, 1519 (1994).
- <sup>13</sup>S. Ishizaka, F. Nihey, K. Nakamura, J. Sone, and T. Ando, *Phys. Rev. B* **51**, 9881 (1995); *Jpn. J. Appl. Phys.* **34**, 4317 (1995).
- <sup>14</sup>H. Xu, *Phys. Rev. B* **50**, 8469 (1994); **50**, 12 254 (1994).
- <sup>15</sup>I. V. Zozulenko, F. A. Maaø, and E. H. Hauge, *Phys. Rev. B* **51**, 7058 (1995).
- <sup>16</sup>G. Kirczenow, *Phys. Rev. B* **46**, 1439 (1992); *Surf. Sci.* **263**, 330 (1992).
- <sup>17</sup>B. L. Johnson and G. Kirczenow, *Phys. Rev. Lett.* **69**, 672 (1992).
- <sup>18</sup>B. L. Johnson, C. Barnes, and G. Kirczenow, *Phys. Rev. B* **46**, 15 302 (1992).
- <sup>19</sup>S. Uryu and T. Ando, *Jpn. J. Appl. Phys.* **34**, 4295 (1995).
- <sup>20</sup>R. L. Schult, D. G. Ravenhall, and H. W. Wyld, *Phys. Rev. B* **39**, 5476 (1989).
- <sup>21</sup>T. Ando, *Phys. Rev. B* **44**, 8017 (1991).
- <sup>22</sup>A. Kumar, S. E. Laux, and F. Stern, *Phys. Rev. B* **42**, 5166 (1990).
- <sup>23</sup>T. Suzuki and T. Ando, *J. Phys. Soc. Jpn.* **62**, 2986 (1993).
- <sup>24</sup>M. C. Gutzwiller, *J. Math. Phys.* **8**, 1979 (1967); **10**, 1004 (1969); **11**, 1791 (1970); **12**, 343 (1971).
- <sup>25</sup>W. H. Miller, *J. Chem. Phys.* **63**, 996 (1975).
- <sup>26</sup>D. Wintgen, *Phys. Rev. Lett.* **61**, 1803 (1988).